

The Influence of Rotor Deflection upon Screw Compressor Performance

Ahmed Kovacevic, MSc, Dipl Ing
Prof Nikola Stosic, PhD, MSc, Dipl Ing,
Prof Ian K. Smith, PhD, MSc, BEng

Centre for Positive Displacement Compressor Technology
City University, London EC1V 0HB, UK; Tel: +44 20 7040 8780; Fax: +44 20 7040 8566
e-mail: a.kovacevic@city.ac.uk

SUMMARY

The compression process within screw compressors induces large pressure and temperature changes that cause the rotors to deform. To determine this effect, a 3-D numerical method has been developed to calculate flow and deformation simultaneously. This comprises a mathematical procedure to generate a numerical grid for both the solid and fluid domains, in the form of a computer program named SCORG, attached to a commercial CCM software package. The effects of rotor distortion on the compressor performance were thus determined and are presented.

NOTATION

ρ	- density	k	- thermal conductivity
p	- pressure	h	- enthalpy
T	- temperature	c_i	- concentration of species
m	- mass	k	- turbulent kinetic energy
V	- cell volume	P	- production of turbulence energy
t	- time	e	- dissipation of turbulent kinetic energy
\mathbf{T}	- stress tensor	C, s	- constants in k - e model of turbulence
\mathbf{S}	- viscous part of the stress tensor	Γ_f	- diffusion coefficient
\mathbf{v}	- velocity		
\mathbf{u}	- deformation		
μ, μ_t	- molecular and turbulent viscosity		
$\mathbf{q}_{fs}, \mathbf{q}_{fv}$	- source terms in transport equations		

INTRODUCTION

Dimensionless or one-dimensional mathematical models are used extensively to predict screw compressor overall performance. These models are based on the assumption of rigid rotors and casing and hence do not account for the effects on performance of rotor deformation, induced by pressure and temperature changes within the machine. This is not

significant when clearances are large. However, screw compressor rotors can now be produced at an economic cost with tolerances as small as 5 micrometers while casing bores can be manufactured on NC machine tools with a repeatability of 2 micrometers. Accordingly it is possible to construct compressors with very small clearances and thereby minimise internal leakage. They may then be made both smaller and more efficient. However, when clearances are small, rotor deformation may affect compressor performance significantly and even lead to seizure. Full 3D calculation of compressor fluid flow and solid structure interaction is then required to evaluate it.

Ferziger and Peric [2] showed that 3-D fluid flow in complex curvilinear geometries can be analysed successfully by means of finite volume methods. *Demirdzic and Muzaferija* [1] showed that by the use of moving frames on structured and unstructured grids, the same numerical methods can be used for the simultaneous solution of fluid flow and structural analysis.

The most extensive descriptions of contemporary grid generation methods are by *Liseikin* [7] and *Thompson et al* [11]. By use of a grid generation procedure based on their methods attached to an appropriate CCM solver, fluid and solid interactions within a system can be predicted.

Apart from the authors' publications [3] - [6], there are hardly any other reported activities in the use of 3D numerical methods for screw compressor studies. This is mainly because existing grid generators and the majority of solvers are still unable to cope with the problems associated with both the complexity of screw compressor geometry and the physics of the compressor process.

The method used in this study employs a rack generation procedure to produce rotor profile points and an analytical transfinite interpolation between them, with adaptive meshing on the boundaries, to obtain a fully structured 3-D computational grid. The authors give this in detail [4]. An interface program called SCORG (**S**crew **C**ompressor **R**otor **G**eometry Grid generator) was developed for this purpose. The grid is directly transferable to a CCM code through its own pre-processor.

Apart from grid generation, some changes need to be made within the solver functions to enable accurate and fast calculations. These include methods to maintain constant pressure at the inlet and outlet ports and the interaction between the solid and fluid domains. An interface program automatically generates user subroutines that contain these features and prepares files to be attached to a general CCM solver.

GRID GENERATION

Grid generation of the screw compressor geometry is a necessary preliminary to CCM calculation. Spatial domains that represent the metal material inside the rotors and the fluid passages outside the rotors should both be defined by it. These are determined by the rotor profile coordinates and their derivatives and are obtained by means of a rack generation procedure described in detail by *Stosic* [9].

An algebraic grid generation method for screw compressor geometry has been derived, based on a transfinite interpolation procedure described by *Liseikin* [7] and *Thompson et al* [11]. This includes stretching functions to ensure grid orthogonality and smoothness, as described by the authors [6]. The compressor spatial domain is divided into a number of sub-domains, which allow the generation of a fully structured grid of discrete volumes within the blocks. A composite grid is then made of several blocks patched together and based on a single boundary fitted co-ordinate system. However, the grid for the fluid around the rotors and the rotors themselves is generated simultaneously in a single block. This allows distortion of the rotors to change the clearances by direct movement of the nodes within the block while the boundary of the block remains unchanged.

MATHEMATICAL MODEL

The compressor flow and the structure of the compressor parts are fully described by the mass averaged conservation equations of continuity, momentum, energy and space, accompanied by the turbulence model equations and an equation of state for the working fluid. These are given by *Ferziger and Peric* [2]. In the case of multiphase flow, a concentration equation is added to the system. The numerical solution of such a system of partial differential equations is then made possible by inclusion of constitutive relations in the form of Stoke's, Fick's and Fourier's law for the fluid momentum, concentration and energy equations respectively and Hooke's law for the momentum equations of a thermo-elastic solid body.

All these equations are conveniently written in the form of the following generic transport equation:

$$\frac{d}{dt} \int_V \mathbf{r} \mathbf{f} dV + \int_S \mathbf{r} \mathbf{f} (\mathbf{v} - \mathbf{v}_s) \cdot d\mathbf{s} = \int_S \Gamma_f \text{grad } \mathbf{f} \cdot d\mathbf{s} + \int_S \mathbf{q}_{fS} \cdot d\mathbf{s} + \int_V q_{fV} \cdot dV \quad (1)$$

Here \mathbf{f} stands for the transported variable and Γ_f is diffusion coefficient. The meaning of the source terms, \mathbf{q}_{fS} and q_{fV} for the fluid and solid transport equations is given in Table 1.

The resulting system of partial differential equations is discretised by means of the finite volume method in a general Cartesian coordinate frame. This method enhances the

conservation of governing equations while at the same time enables a coupled system of equations to be solved simultaneously for both the solid and fluid regions.

Table 1 Terms in the generic transport equation (1)

Equation	f	Γ_f	q_{fs}	q_{fv}
Fluid Momentum	v_i	μ_{eff}	$\left[\mathbf{m}_{eff} (\text{grad } \mathbf{v})^T - \left(\frac{2}{3} \mathbf{m}_{eff} \text{div } \mathbf{v} + p \right) \mathbf{I} \right] \cdot \mathbf{i}_i$	$f_{b,i}$
Solid Momentum	$\frac{\partial u_i}{\partial t}$	η	$\left[\mathbf{h} (\text{grad } \mathbf{u})^T + (\mathbf{I} \text{div } \mathbf{u} - 3K\alpha\Delta T) \mathbf{I} \right] \cdot \mathbf{i}_i$	$f_{b,i}$
Energy	e	$\frac{k}{\partial e / \partial T} + \frac{\mathbf{m}}{\mathbf{s}_T}$	$-\frac{k}{\partial e / \partial T} \frac{\partial e}{\partial p} \cdot \text{grad } p$	$\mathbf{T} : \text{grad } \mathbf{v} + h$
Concentration	c_i	$\mathbf{r} D_{i,eff}$	0	s_{ci}
Space	$\frac{1}{\mathbf{r}}$	0	0	0
Turbulent kinetic energy	K	$\mathbf{m} + \frac{\mathbf{m}}{\mathbf{s}_k}$	0	$P - \mathbf{re}$
Dissipation	\mathbf{e}	$\mathbf{m} + \frac{\mathbf{m}}{\mathbf{s}_e}$	$C_1 P \frac{\mathbf{e}}{k} - C_2 \mathbf{r} \frac{\mathbf{e}^2}{k} - C_3 \mathbf{re} \text{div } \mathbf{v}$	

This mathematical scheme is accompanied by boundary conditions for both the solid and fluid parts. The authors [5] introduced special treatment of the compressor fluid boundaries. The compressor was positioned between two relatively small suction and discharge receivers. By this means, the compressor system is separated from the surroundings by adiabatic walls only. It communicates with its surroundings through the mass and energy sources or sinks placed in these receivers. This way of maintaining constant suction and discharge pressures is given by the authors [6]. The solid part of the system is constrained by both Dirichlet and Neuman boundary conditions through zero displacement in the restraints and zero traction elsewhere. Connection between the solid and fluid parts is determined explicitly through the energy equation if the temperature and displacement from the solid body surface are boundary conditions for the fluid flow and vice versa.

A commercial CCM solver was used to obtain the distribution of pressure, temperature, velocity and the density fields throughout the fluid domain as well as the deformation and stresses of the solid compressor elements. Based on the solution of these equations, integral parameters of screw compressor performance were calculated, as shown by *Kovacevic et. al.* [6] and *Stosic et. al.* [10].

PRESENTATION AND DISCUSSION OF THE RESULTS

Interaction between the fluid flow and the solid parts is analysed in this paper for three common applications of screw compressors, each with the same geometry, as shown in Figure 1.

These are: an oil-injected air compressor of moderate pressure ratio, a dry air compressor, in which the pressure ratio is low, and a high pressure oil flooded compressor. In all three cases, the rotor profiles are of the 'N' type with a 5/6 lobe configuration, as presented by *Stosic et. al.* [8]. The rotor outer diameters are 128 and 101 mm for the male and female rotors respectively, and their centre distance is 90 mm. The rotor length to diameter ratio is 1.65. The numerical mesh for the test case in this study comprises 513,617 cells of which 162,283 describe the solid part of the rotors, 189,144 other cells map the fluid parts between the rotors while the rest specify the suction and discharge ports and oil openings. A cross section through the mesh for the rotors and their fluid paths is presented in Figure 2.

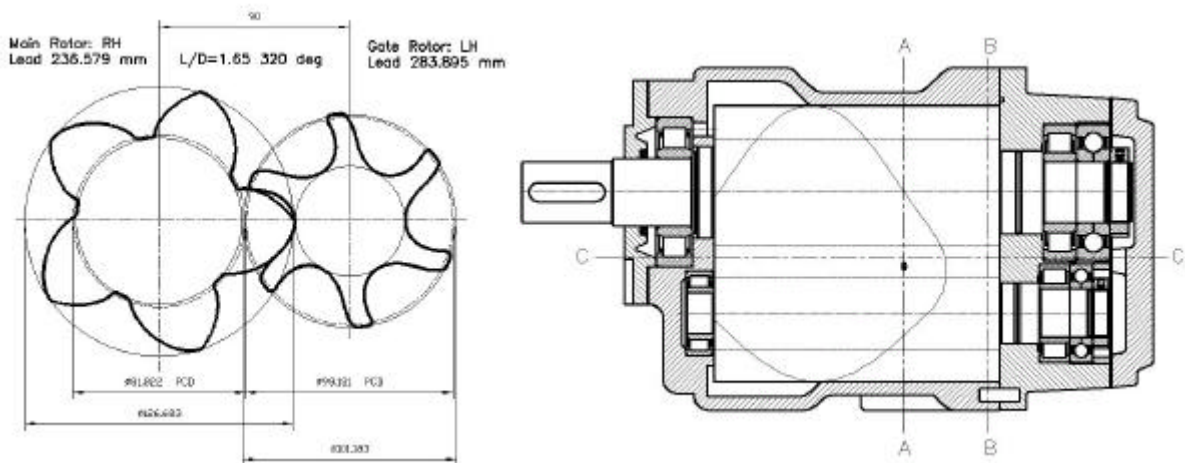


Figure 1 Cross section of rotors (left) and compressor (right)

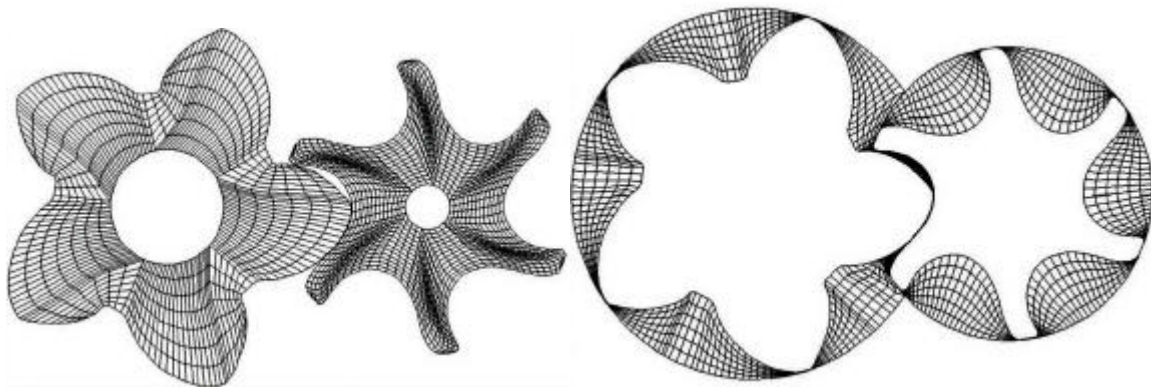


Figure 2 Numerical mesh for rotors (left) and their fluid parts (right)

The grid and other control parameters generated by the interface were applied to COMET, a commercial CCM solver of the StarCD group. The calculations were carried out on a computer powered by an Athlon 800 MHz processor and 1 GB memory. Compressor rotation

was simulated by means of 24 time steps for one interlobe rotation. This was equivalent to 120 time steps for one full rotation of the male rotor. The time step length was synchronised with a compressor speed of 5000 rpm. An error reduction of 4 orders of magnitude was required, and achieved within approximately 50 outer iterations at each time step. One time step took approximately 30 minutes of computer time.

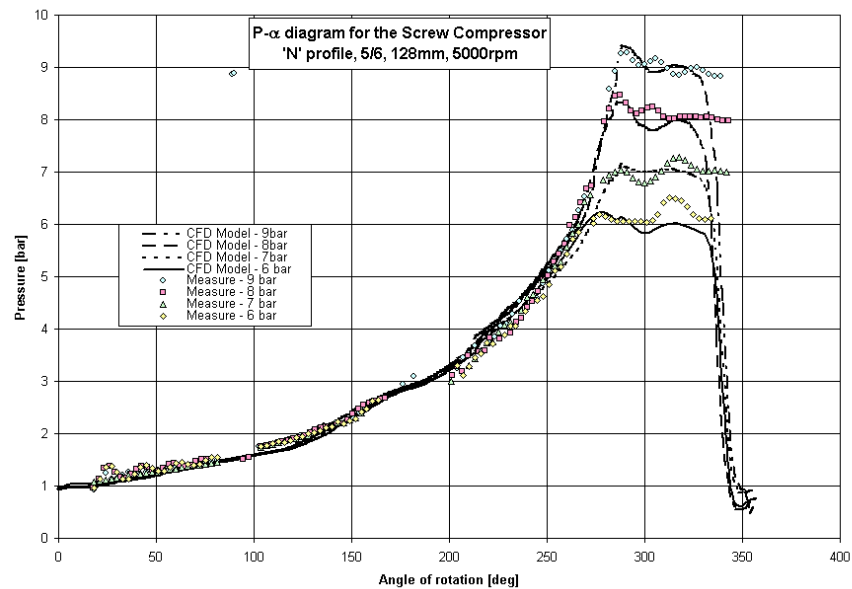


Figure 3 Pressure-shaft angle diagram; comparison of CFD calculations and measurements

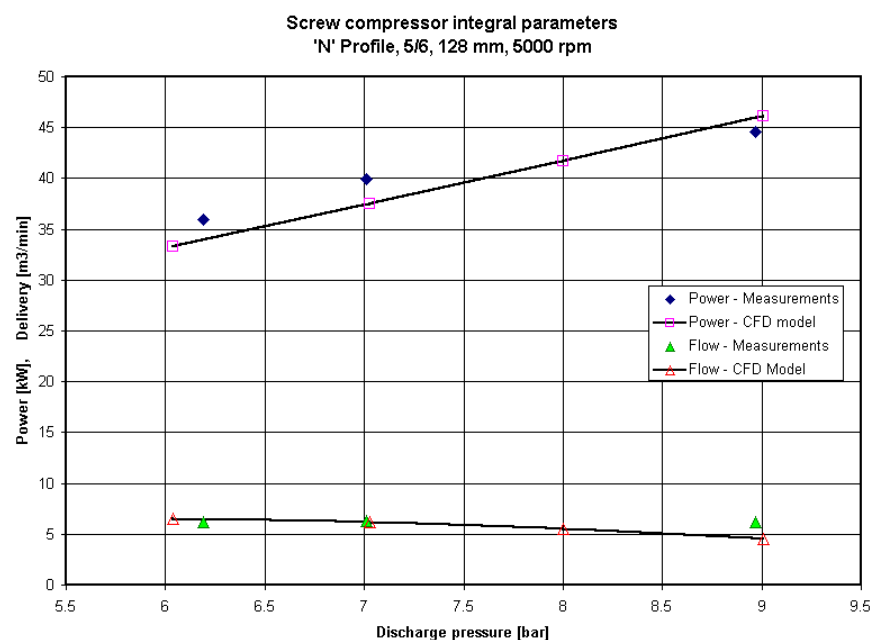


Figure 4 Comparison of integral results obtained by measurements and modelling

In the case of the oil injected air compressor, the results of the 3D calculations were compared with measurements obtained from an experimental compressor of identical

dimensions. The pressure fluctuations within the machine were measured with piezoresistive transducers, positioned in the male rotor side of the housing to cover as much as possible of the whole process. Measured results were obtained for suction conditions of 1 bar abs pressure and 20°C temperature with discharge pressures of 6, 7, 8 and 9 bar. The results are compared with the numerical simulations. Good agreement was obtained both for instantaneous values shown in Figure 3 and integral parameters shown in Figure 4.

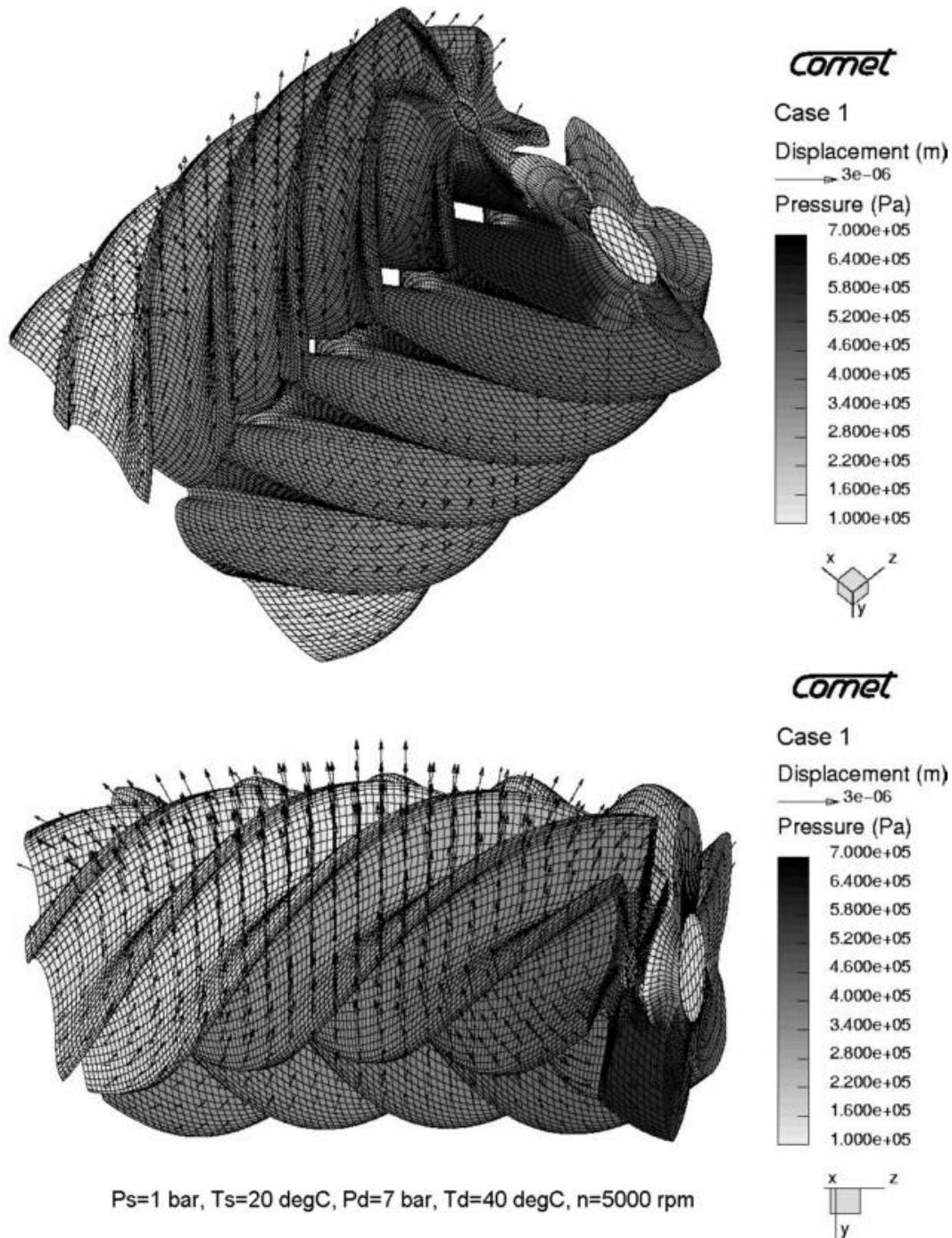
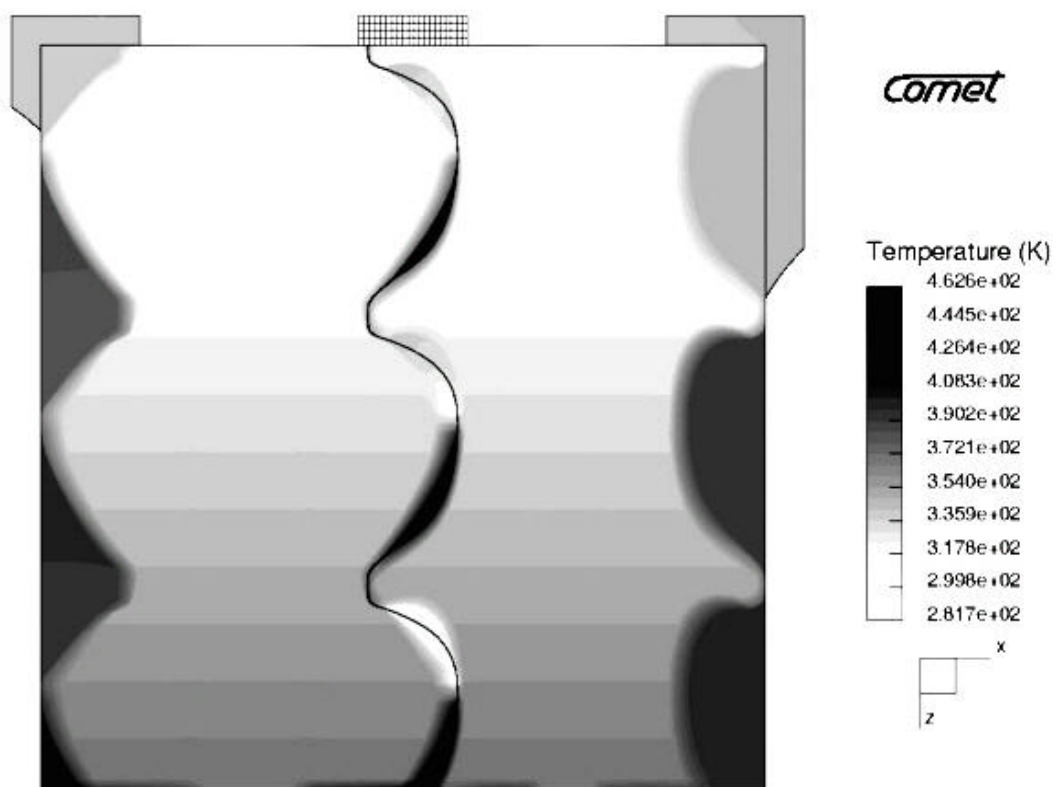


Figure 5 Displacement vectors and the acting pressure on deformed rotors for oil injected compressor

The average exit temperature from the compressor was maintained at 40 °C at all pressures by suitable injection of oil. Consequently, the rotor deformation was caused mainly by the pressure rise in the working chamber. Two views of the rotors are presented in Figure 5, one from the bottom of the rotors and the other one from the female rotor side. How the pressure forces push the rotors apart and bend them has been made visible in the top diagram by magnifying the distortion 20,000 times while maintaining the other dimensions at their original scale. The leakage path through the sealing line between the rotors is biggest on the discharge side where the pressure difference between the two rotors is the greatest. Also, rotor bending increases the clearance gap between the rotor and the housing on the back wall of the compressor. The female rotor is weaker than the male and therefore deforms more. The maximum deformation in this case is only a few micrometers

The oil free air compressor works between suction conditions of 1 bar and 20°C and a discharge pressure of 3 bar. Due to the lack of cooling oil, the temperature rise in the compressor is much greater and has an average value of 150°C at the discharge port. The deformation in this case is presented in Figure 6. Here, the effects of pressure difference are negligible compared to the deformation caused by the temperature change, which has the effect of enlarging the rotors, especially in the discharge area. The fluid temperature in the immediate vicinity of the solid boundary changes rapidly, as shown in the bottom diagram. However, the temperature of the rotor pair is lower due to the continuous averaging oscillations of pressure and temperature in the surrounding fluid. This is shown in the top diagram of Figure 6, where the temperature distribution is given in cross section for both the fluid flow and the rotor body. The deformation, presented in the bottom of the figure, is increased 1,500 times in order to make it visible. It has a maximum value of 50 μ m, which is more than an order of magnitude greater than in the case of the oil flooded compressor. The rotor working clearances are thus reduced by the same amount. By this means leakage flow in the most critical areas is reduced. However, in the design of the dry screw compressor, sufficient initial clearance should be allowed to prevent distortion causing rotor seizure.

The high pressure oil injected application was taken as a CO₂ refrigeration compressor with suction conditions of 30 bar and 0°C and discharge conditions of 90 bar and 40°C. In this case, the large pressure difference was the main cause of the rotor deflection with the highest deformation in excess of 15 μ m, as shown in Figure 7. The deformation pattern of the rotors is similar to the low pressure case but with slight enlargement at discharge.



Ps=1 bar, Ts= 20 degC, Pd=3 bar, Td=150 degC, n=5000 rpm

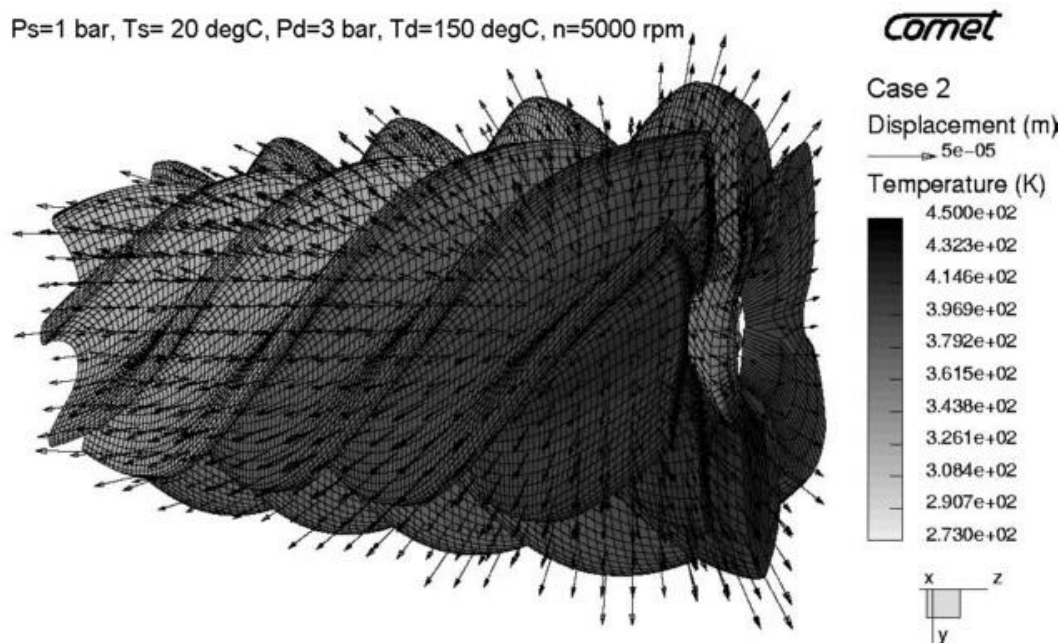


Figure 6 Rotor displacement vectors and temperature distribution for an oil free compressor

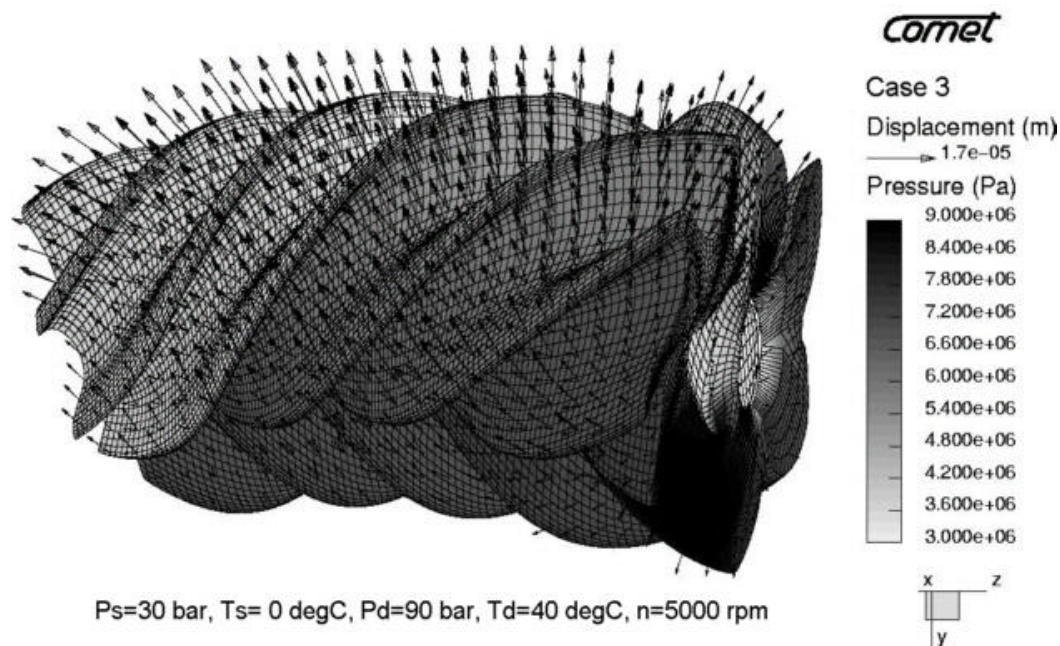


Figure 7 Deformations of a high pressure oil injected compressor

The change of clearance caused by rotor deformation affects the compressor integral parameters, as shown in Figure 8. The reduced rotor clearance due to the temperature dilatation increases both the compressor flow and power input. However, the effect on the flow is greater than on the power and hence the specific power decreases, or more conventionally, the efficiency increases. In the other cases, the rotor deflections caused by the pressure enlarge the clearances. For a moderate pressure rise, the effect on delivery and power consumption is negligible. In the CO₂ refrigeration application, the rotors deform more and the decrease in delivery and rise in specific power becomes more pronounced.

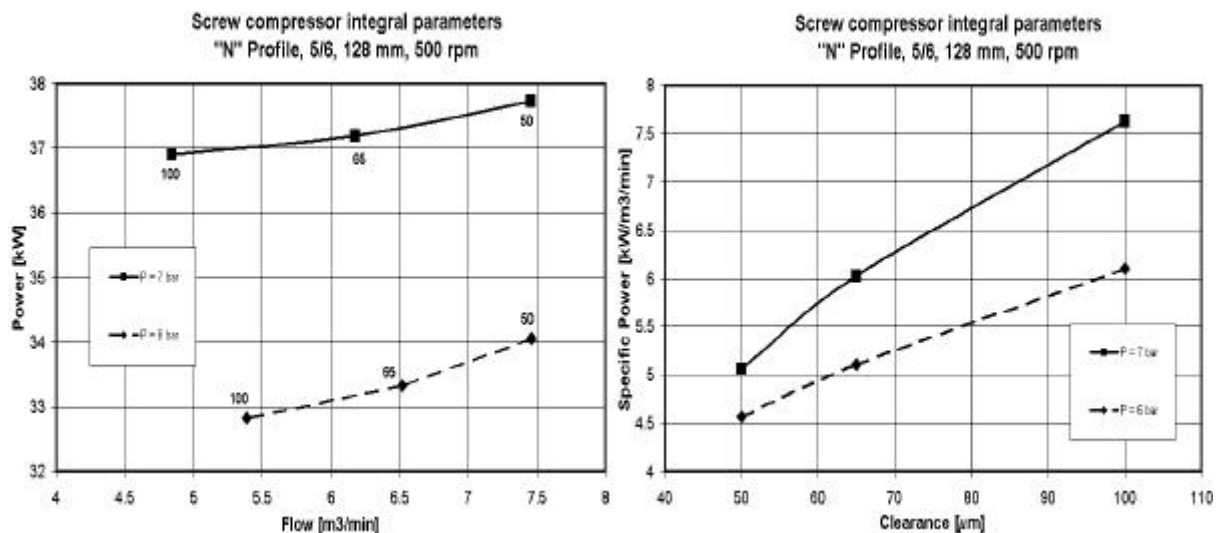


Figure 8 Influence of the rotor deflection to the integral compressor parameters

CONCLUSIONS

A full 3-D simulation has been carried out to determine how pressure and temperature changes create internal distortion within screw compressors and thus affect their performance. The effects of the change in working clearances are compared for different compressor applications and presented through distortion diagrams and flow-power charts. A high pressure rise has adverse effects but a high temperature rise may lead to an increase in delivered flow and efficiency. As is shown in the results, the rotor deformation is dependent on the compressor application. It must, therefore, be taken into account in every specific compressor design.

REFERENCES

1. Demirdzic, I., Muzaferija S., "Numerical Method for Coupled Fluid Flow, Heat Transfer and Stress Analysis Using Unstructured Moving Mesh with Cells of Arbitrary Topology", *Comp. Methods Appl. Mech Eng*, 1995, Vol. 125, pp 235-255
2. Ferziger, J.H., Peric, M.; "Computational Methods for Fluid Dynamics", Springer, Berlin, Germany, 1996
3. Kovacevic, A.; Stosic, N.; Smith, I.K.; "The CFD Analysis of a Screw Compressor Suction Flow", 2000 International Compressor Conference at Purdue University, West Lafayette, Indiana, July 2000, pp 909-916
4. Kovacevic, A., Stosic, N.; Smith, I.K.; "Grid Aspects of Screw Compressor Flow Calculations", *Proceedings of the ASME International Mechanical Engineering Congress*, Orlando, Florida, November 2000, pp 79-82
5. Kovacevic, A.; Stosic, N.; Smith, I.K.; "Analysis of Screw Compressor by Means of Three-Dimensional Numerical Modelling", *International Conference on Compressor and their System*, IMechE Conference Transactions 2001-7, London, 2001, p.23-32
6. Kovacevic, A.; Stosic, N.; Smith, I.K.; "CFD Analysis of Screw Compressor Performance ", In: "Advances of CFD in Fluid Machinery Design" edited by Elder, R.L, Tournlidakis, A, Yates M.K, Professional Engineering Publishing of ImechE, London, 2002
7. Liseikin, V.D., "Grid generation Methods", Springer-Verlag, 1999
8. Stosic, N.; Smith, I.K.; Kovacevic, A, Aldis C.A., "The Design of a twin-screw compressor based on a new rotor profile", *Journal of Engineering Design*, v.8, n.4 1997, pp 389-399
9. Stosic, N.; "On Gearing of Helical Screw Compressor Rotors", *Proc IMechE, Journal of Mechanical Engineering Science*, 1998, Vol.212, pp 587
10. Stosic, N, Hanjalic K., "Development and Optimization of Screw Machines with a Simulation Model, Part I: Profile Generation, Part II: Thermodynamic Performance Simulation and Design", *ASME Proceedings, Journal of Fluids Engineering*, 1997, Vol 119, p 659, p664
11. Thompson, J.F; Soni, B.; Weatherrill, N.P.; "Handbook of Grid generation", CRC Press 1999